

Particle-in-Cell simulation of two-dimensional electron velocity shear driven instability in relativistic domain

Chandrasekhar Shukla* and Amita Das†

Institute for Plasma Research, Bhat , Gandhinagar - 382428, India

Kartik patel

Bhabha Atomic Research Centre, Trombay, Mumbai - 400 085, India

(Dated: May 31, 2016)

Abstract

We carry out Particle-in-Cell (PIC) simulations to study the instabilities associated with a 2-D sheared electron flow configuration against a neutralizing background of ions. Both weak and strong relativistic flow velocities are considered. In the weakly relativistic case, we observe the development of electromagnetic Kelvin Helmholtz instability with similar characteristics as that predicted by the electron Magnetohydrodynamic (EMHD) model. On other hand, in strong relativistic case the compressibility effects of electron fluid dominate and introduce upper hybrid electrostatic oscillations transverse to the flow which are very distinct from EMHD fluid behaviour. In the nonlinear regime, both weak and strong relativistic cases lead to turbulence with broad power law spectrum.

* chandrasekhar.shukla@gmail.com

† amita@ipr.res.in

I. INTRODUCTION

The fundamental physical processes which governs the evolution of electron flows with velocity gradient are of great interest in wide range of research areas in astrophysical and laboratory contexts. In astrophysical scenario, the relativistic jets which are observed across wide range of astrophysical scales from micro-quasars to Gamma Ray Bursts (GRBs), supernovas etc., [1–4] would have sheared flow of electrons. In laser plasma experiments also, there are many situations where the sheared electron flow configuration is inevitable. For instance experiments on fast-ignition scheme of laser-driven inertial confinement fusion involve electron beam propagation inside a plasma which would invariably result in a sheared configuration of electron flow. When a high intensity laser irradiates a solid surface and/or a compressed plasma it generates electron beam at the critical density surface of the plasma by the wave breaking mechanism [5–7]. This beam typically propagates inside the high density region of the plasma exciting reverse shielding background electron currents. The forward and reverse currents spatially separate by Weibel instability leading to a sheared electron flow configuration. However, since the transverse extent of the beam is finite compared to the plasma width, being commensurate with the laser focal spot, the sheared configuration of electron flow automatically exists between the beam and the background stationary electrons at the edge of the propagating beam [8] even before Weibel destabilization process. In such a scenario the Kelvin-Helmholtz (KH) instability develops immediately at the edge of the beam and does not require a Weibel destabilization process to preempt it.

The KH instability is a well known instability and has been widely studied in the context of hydrodynamic fluid. However, the sheared-electron velocity flow encountered in laboratory and astrophysical cases, mentioned above, differs from the hydrodynamic fluid flows in many respects. For instance, the sheared-flow configuration of electron fluid invariably has currents and sheared current flows associated with it. Consequently, the evolution of the magnetic field associated with it becomes an integral part of the dynamics. Development of charge imbalance is another aspect in the evolution. Though the equilibrium charge balance is provided by the neutralizing static background of electrons, compressible electron flow during evolution can easily lead to charge imbalance as the ions would not respond at fast electron time scale phenomena. This would lead to electrostatic field generation which has added influence in the dynamics. Lastly, the flow of electrons in most cases is relativistic.

Thus, to summarize the KH instability in this case has additional effects due to the presence of electromagnetic features, compressibility leading to electrostatic fields, relativistic effects etc. In the non-relativistic limit the electromagnetic effects on KH instability in the context of sheared electron flows have been investigated in detail by employing the Electron Magnetohydrodynamic (EMHD) model [16–19]. This model neglects the displacement currents and space charge effects and assumes stationary ions which provide the neutralizing background. The relativistic effects on K-H instability in compressible neutral hydrodynamic fluid has been studied by Bodo *et al.* [12, 13]. Recently,[20] Sundar *et al.* have incorporated relativistic effects on sheared-electron flows. This study points out crucial role of shear on the relativistic mass factor due to sheared velocity configuration. The effect due to displacement current was retained in the relativistic regime. It was, however, shown that for the weakly relativistic case the effects due to displacement current were negligible. However, in these studies, the space charge effects which may arise when compressibility of the electron fluid are present, have not been incorporated. The present article aims at exploring these features using a PIC simulation.

We have carried out a 2.5D relativistic electromagnetic Particle-in-Cell simulations to study the electron shear flow instability in both cases of weak and strong relativistic flows. By 2.5D we mean that all three components of the fields are taken into consideration, however, their spatial variations are confined in 2-D plane only. When the flow is weakly relativistic, we observe the development of electromagnetic KH instability at the location of shear which ultimately develops into vortices. These vortices merge subsequently forming longer scales, in conformity with the inverse cascade phenomena observed in typical 2-D fluid systems. The density perturbations are observed to be weak in this case. The results in this case are thus very similar to the predictions of the EMHD fluid behaviour. When the relativistic effects are mild (and not weak), the KH instability occurs at a slower time scales. The KH vortices are observed initially, which are soon overwhelmed by compressibility effects which introduce magnetized non-linear electrostatic oscillations (non-linear upper hybrid oscillations) in plasma transverse to flow. In strongly relativistic regime the electrostatic oscillations dominate right from the very beginning. The amplitude of the oscillations increases leading to phenomena of wave breaking. In the nonlinear regime, the spectra is observed to be broad in all the three cases which implies turbulence.

The paper is organized as follows. In section II, we describe our simulation methodology.

The results of PIC simulations and their implications are presented in section III. It is seen that in strong relativistic case compressibility effects seem to dominate resulting in electrostatic oscillations transverse to the flow. These electrostatic oscillations are understood on the basis of a simplified one dimensional model in section IV. Section V contains the description of the power spectrum of the fields in the nonlinear regime. Section VI contains the summary and conclusions.

II. DESCRIPTION OF SIMULATION

We choose the electron to have a flow velocity along \hat{y} with a following sheared flow configuration as equilibrium

$$V_{0y}(x) = V_0 [\tanh((x - L_x/4)/\epsilon) + \tanh((3L_x/4 - x)/\epsilon)] - V_0, \quad (1)$$

where ϵ is width of shear layer, L_x is total length of simulation box in transverse direction of flow and V_0 is the maximum amplitude of the flow velocity. This flow structure is shown schematically in Fig. 1. The electron flow is responsible for current and produces an equilibrium magnetic field in the $B_0\hat{z}$ direction. During the simulations, ions are kept at rest and merely provide for the neutralizing background. In order to satisfy the condition for equilibrium force balance on electrons, there is a need to displace the electrons and ions slightly in space, so that an equilibrium electric field \vec{E}_0 gets created. This is chosen in such a fashion so as to satisfy the condition of

$$\vec{E}_0 + \frac{V_{0y}\hat{y} \times \vec{B}_0\hat{z}}{c} = 0 \quad (2)$$

This ensures that the Lorentz force on electrons vanishes everywhere. This clearly indicates the necessity for having an equilibrium electric field along \hat{x} . The electron and ion charges are thus displaced in an appropriate fashion so as to satisfy the Gauss's law

$$\nabla \cdot \mathbf{E} = \frac{\partial E_x}{\partial x} = -\frac{1}{c} \frac{\partial (B_{0z} V_{0y})}{\partial x} = 4\pi e (n_{0i} - n_{0e}), \quad (3)$$

here n_{0i} and n_{0e} are unperturbed ion and electron number densities respectively in equilibrium, e is charge of electron and c is speed of light. To maintain equilibrium in system we have thus arranged the electron particle number density according to following relationship [22],

$$n_{0e} = n_{0i} + \frac{1}{4\pi e c} \frac{\partial (B_{0z} V_{0y})}{\partial x}. \quad (4)$$

The ions are distributed uniformly with a density n_{0i} of $3.18 \times 10^{18} \text{cm}^{-3}$ and n_{0e} is adjusted as per Eq. (4). The area of the simulation box R is chosen to be $6 \times 5 (c/\omega_{0e})^2$ corresponding to 600×500 cells; where $\omega_{0e} = \sqrt{4\pi n_{0i} e^2 / m_e}$ is electron plasma frequency corresponding the uniform plasma at the background density of ions. Also, $c/\omega_{0e} = d_e = 3.0 \times 10^{-4} \text{cm}$ is the skin depth. We have used 128 particles per cell for both ion and electron in our simulation. To resolve the underlying physics at the scale which is smaller than the skin depth, we have chosen a grid size of $0.01d_e$. The time step Δt , decided by the Courant condition, is 0.035 femtosecond.

We have considered four different set of parameters for our investigation. In all cases, velocity profile of electron is assigned by eq. 1. For the first case, we choose the flow velocity of electron in the weakly relativistic regime and chose the shear width to be less than the plasma skin depth. We would refer this as Case (a) which has the following parameters $V_0 = 0.1c$, $\epsilon = 0.05 c/\omega_{0e}$. This is the weakly relativistic case where the EMHD fluid description is supposed to work pretty well. We consider then in case (b), the dependence of KH instability on shear width. We do this by changing the value of shear width in comparison to skin depth. As per the EMHD description the growth rate decreases when the shear width is shallow compared to the skin depth. We illustrate this by specifically choosing a value of $\epsilon = 1.5 c/\omega_{0e}$. In the third and fourth cases (c) and (d) a mild and strong relativistic limit with parameters $V_0 = 0.5c$, $\epsilon = 0.05 c/\omega_{0e}$ and $V_0 = 0.9c$, $\epsilon = 0.05 c/\omega_{0e}$ are respectively considered.

III. PIC SIMULATION RESULTS

In the three subsections we discuss the results of (I) Weakly relativistic (II) Mild relativistic (III) Strong relativistic cases.

A. I. Weakly relativistic

We choose a the value of $V_0 = 0.1c$ for electron velocity to study the weakly relativistic case. We observe a destabilization of the sheared flow configuration. The instability is tracked by plotting the evolution of the perturbed kinetic energy(PKE) of the electrons in the system. This is shown in Fig. 2. The initial steep rise is due to numerical noise.

Thereafter, the instability grows from the noise spectrum. Since, the noise would lack the exact eigen mode structure of any particular mode, initially a combination of unstable modes start growing. Subsequently, as the mode with fastest growth dominates a linear rise in the plot of PKE can be clearly observed. It should be noted that evolution follows the EMHD fluid predictions of the growth rate being higher for the case (a) when the shear width is sharper than the skin depth. In case (b) the growth is observed to be small and the saturation also occurs quite fast.

For a closer look at the instability development the color contour plot of the evolution of magnetic field (Fig. 3), vorticity (Fig. 5) and the two components of Electric field (Fig. 4) has been shown at various times. From (Fig. 3) magnetic field evolution, one can observe that the magnetic perturbations start at the location where velocity shear is maximum. These perturbations grow forming magnetic vortices which subsequently merge to form bigger structures. The merging process of magnetic field is along expected lines of 2-D inverse cascade EMHD depiction of the problem. The fluid vorticity also shows similar traits, however, at later times $t = 59.60$ (in normalized units) the long scale vorticities show signs of disintegration. The two components of electric fields also show emergence of KH structures and merging. A comparison of normalized amplitudes of electric and magnetic field shows that the electric fields are much weaker than the magnetic fields. We also show the plot of electron density in the nonlinear regime of the KH instability at $t = 36.75$ in Fig. 6. We observe that the density also acquires distinct structures of KH like vortices in the shear region. The density perturbations in the weakly relativistic case is observed to be weak. The maximum observed value of $\tilde{n}e/n_{e0} \sim 1.2$. On the other hand we would see in the strongly relativistic case this is as large as 8 to 10. This suggests that in the weakly relativistic regime the instability essentially has an electrostatic character.

B. II. Mild relativistic case

In the mild relativistic case where $V_0 = 0.5c$, the KH is observed to be considerably weak. The vorticity plots shown in Fig. 8 shows an initial tendency towards developing the KH rolls. The KH rolls in this case are fewer in number. For case(a) they were 5 here they are only around 3. This again suggests that the growth rate for relativistic case gets confined towards longer scale as per the predictions of EMHD model. The fluid analysis carried out

earlier also suggests that the cut off wavenumber of the KH moves towards longer scales in mildly relativistic cases.

The KH rolls are observed to be very soon overwhelmed by certain oscillations transverse to the flow. The oscillations transverse to the flow are also clearly evident in the electron density plots of Fig. 7. The density oscillations in this case are pretty strong with $\tilde{n}_e/n_{e0} \sim 4$. The KH suppression and the appearance of these upper electrostatic oscillations can be understood as follows. As the relativistic effect increases the $\vec{V} \times \vec{B}/c$ force becomes dominating. Thus a small perturbed magnetic field \tilde{B} , induces a strong $V_0 \times \tilde{B}/c$ force along x , which is responsible for the upper hybrid electrostatic oscillations.

C. III. Strong relativistic

We now choose $V_0 = 0.9c$ for understanding the strongly relativistic case. The time evolution of PKE in this case shows the linear growth of the instability. However, the instability is dominated by the upper hybrid electrostatic oscillations which are observed right from the very beginning. Thus the development of the rolls typical of the KH instability are not very clearly evident in this case. Representing the initial distribution of flowing and the static electrons by different colors (red and blue respectively) we show the snapshots of their displacement in space in Fig. 9. The electron compressibility is clearly evident, so much so and white regions devoid of electrons are created (snapshot at $\omega_{0e}t = 3.5$). The Electric fields due to background ions, however, pull these electrons back which results in a large amplitude excitation of nonlinear upper hybrid electrostatic plasma oscillations. These oscillations are discussed in detail in the next section.

A comparative value of the growth rate obtained from the slope of the evolution of PKE in the table below for all the cases studied by us.

TABLE I

The maximum growth rate (Γ_{grmax}) of K-H instability evaluated from slope of perturbed kinetic energy

V_0/c	$\varepsilon/(c/\omega_{0e})$	$\Gamma_{max}/(V_0\omega_{0e}/c)$
0.1	0.05	0.7
0.1	1.5	0.0
0.5	0.05	0.34
0.9	0.05	0.23

Since, classically the KH instability typically scales with the fluid flow velocity we have chosen to divide the growth rate with V_0 for a better appreciation of the comparison. The comparison clearly, shows that Γ_{max}/V_0 decreases due to relativistic effects in agreement with the earlier fluid analysis by Sundar *et al.* Thus the distinction between the PIC and EMHD fluid simulations finally boils down to the appearance and dominance of electrostatic oscillations transverse to the flow direction. We study the transverse oscillations in detail in the next section.

IV. NONLINEAR UPPER HYBRID ELECTROSTATIC OSCILLATIONS

One of the main observations is the appearance of strong upper hybrid electrostatic oscillations triggered from the edge of the flow region with increasing relativistic effects. We show in Fig. 10 the amplitude of these oscillations as a function of time at $y = 2.5 c/\omega_{0e}$ for the strongly relativistic case of $V_0 = 0.9c$. It can be seen that the density perturbations acquire a very high amplitude fairly rapidly $\tilde{n}_e/n_{e0} \sim 8$. This is a very nonlinear regime for the oscillations where wave breaking and trajectory crossing would occur. This is indeed so as the particle distribution of Fig. 9 shows clear crossing of blue and red electrons.

In order to understand the dynamics behind this phenomenon, we model the phenomena by a one-dimensional magnetized relativistic electron fluid equations for electrostatic disturbances. Thus the governing equations of the model are expressed as

$$\left(\frac{\partial}{\partial t} + v_{ex}\frac{\partial}{\partial x}\right)n_e = -n_{ex}\frac{\partial v_{ex}}{\partial x}, \quad (5)$$

$$\left(\frac{\partial}{\partial t} + v_{ex}\frac{\partial}{\partial x}\right)p_{ex} = -eE_x - \frac{ev_{ey}B_0(x)}{c}, \quad (6)$$

$$\left(\frac{\partial}{\partial t} + v_{ex}\frac{\partial}{\partial x}\right)p_{ey} = \frac{ev_{ex}B_0(x)}{c}, \quad (7)$$

$$\left(\frac{\partial}{\partial t} + v_{ex}\frac{\partial}{\partial x}\right)E_x = 4\pi en_{0i}v_{ex}, \quad (8)$$

$$(9)$$

where $p_{e\alpha} = \gamma m_e v_{e\alpha}$ is α -component of momentum; α is subscript for x and y, $\gamma = [1 + p^2/m_e^2 c^2]^{1/2}$ is relativistic factor and n_{0i} is background ion density. The inhomogeneous magnetic field $B_0(x)$ is the equilibrium magnetic field generated from the equilibrium electron flow considered in our PIC simulations. For the double tangent hyperbolic profile it will have the following form:

$$B_0(x) = \frac{4\pi n_{0e} e}{c} (V_0 \epsilon \log(\cosh(0.25L_x - x)) + V_0 \epsilon \log(\cosh(x - 0.75L_x)) - V_0 x). \quad (10)$$

We have solved the above equations numerically with initial profile of v_{ey} using the eq. (1). For the weakly relativistic case of $V_0 = 0.1c$ the electrostatic oscillations that get generated are quite small and continue to remain so indefinitely (See Fig. 11). However, when the value of V_0 is increased to a high value of $V_0 = 0.9c$, large-amplitude non-linear oscillations in electron density (see Fig. 12) can be clearly seen. This is similar to the results of our PIC simulations.

The upper hybrid frequency ω_{UH} is given by

$$\omega_{UH}^2 = \omega_{0e}^2 + \omega_{ce}^2 \quad (11)$$

In our simulations, since the magnetic field is nonuniform, the upper hybrid oscillations occur against an inhomogeneous magnetic field background. For comparing the observed oscillation frequency with that of the upper hybrid oscillations we have chosen to consider an average magnetic field. Thus $\omega_{ce} = eB_{r.m.s}/m_e c$, $B_{r.m.s}$ is root mean square value of magnetic field. We calculate the upper hybrid frequency from dispersion relation eq. 11, from PIC simulation of ω_{UH} and from 1D model and have tabulated it in table II for the two cases of mild and strong relativistic flows. It can be seen that all the two approaches (simplified dispersion equation and 1 D model) yield comparable estimates for the observed electrostatic oscillations in the PIC simulations.

TABLE II

The table for upper hybrid frequency obtained from dispersion relation eq. 11 $\omega_{UH}(anal.)$, from PIC simulation $\omega_{UH}(PIC)$ and from 1d model $\omega_{UH}(1d \text{ model})$ for various different value of V_0

V_0/c	$\omega_{UH}(anal.)/\omega_{0e}$	$\omega_{UH}(PIC)/\omega_{0e}$	$\omega_{UH}(1d\ model)/\omega_{0e}$
0.5	1.09	1.06	1.06
0.9	1.27	1.26	1.25

The upper hybrid frequency obtained from various method are match very well and affirm the existence of upper hybrid mode in sheared electron flow.

V. NONLINEAR REGIME

The nonlinear regime of the simulation shows evidence of turbulence generation for both weak and strong relativistic cases. We have plotted the spectra of magnetic and electric fields as a function of k_y defined by the following relationship.

$$S_F(k_y) = \frac{1}{L_x} \int_0^{L_x} F^2(x, k_y) dx, \quad (12)$$

where $S_F(k_y)$ is one dimensional longitudinal energy spectra of the field F, where F is the x- dependent longitudinal Fourier transform of any of the electric and magnetic fields (represented by R here) given by

$$F(k_y, x) = \frac{1}{L_y} \int_0^{L_y} R(x, y) \exp(-ik_y y) dy, \quad (13)$$

We observe that in both strong and weak relativistic cases the spectra is broad and has a power law behaviuor (see Fig. 15, Fig. 13 and Fig. 14). The spectral scaling index is found to be close to -4 . In the strong relativistic case, we observe that the power law extends towards the longer wavelength region of $kd_e \sim 1$ whereas this is not so for the weak relativistic case. It appears that it is easier to generate longer scales in the strongly relativistic case.

VI. SUMMARY AND CONCLUSION

A detailed PIC simulation was carried out to study the instability of sheared relativistic electrons against a background of neutralizing ions. Our studies on weakly relativistic case show good agreement with the observations based on EMHD fluid approximation. For instance the observation of instability getting driven when the shear scale is sharper than the skin depth, the development of KH vortices in the shear region which ultimately merge

to form longer structures etc., are all in conformity of the fluid EMHD theory. In the strong relativistic case the compressibility effects are dominant and one observes a characteristic electrostatic oscillations transverse to the flow direction. This overwhelms the KH in the system. The nonlinear regime in all cases shows a broad power spectra of magnetic field which is indicative of turbulence.

-
- [1] A.Thiessen.G.B.Zimmerman J.H.Nuckolls, L.Wood, *Nature* **239**, 139 (1972).
- [2] Yosuke Mizuno, Philip E. Hardee, and Ken-Ichi Nishikawa, *ApJ* **784**, 167 (2014).
- [3] Ken-Ichi Nishikawa *et al.*, *Ann. Geophys.* **31**, 1535 (2013).
- [4] R. A. Chevalier, J. M. Blondin, and R. T. Emmering, *ApJ* **392**, 118 (1992).
- [5] G. Malka and J. L. Miquel, *Phys. Rev. Lett.* **77**, 75 (1996).
- [6] A. Modena, *Nature* **377**, 606 (1995).
- [7] K. B. Wharton, S. P. Hatchett, S. C. Wilks, M. H. Key, J. D. Moody, V. Yanovsky, A. A. Offenberger, B. A. Hammel, M. D. Perry, and C. Joshi, *Phys. Rev. Lett.* **81**, 822 (1998).
- [8] Chandrasekhar Shukla, Amita Das and Kartik Patel, *arxiv.org* (2015).
- [9] Erich S. Weibel, *Phys. Rev. Lett.* **2**, 83 (1959).
- [10] Burton D. Fried, *Physics of Fluids* **2**, 337 (1959).
- [11] Y. Sentoku, K. Mima, P. Kaw, and K. Nishikawa, *Phys. Rev. Lett.* **90**, 155001 (2003).
- [12] P. G. Drazin and W. H. Reid, *Hydrodynamic Stability* (Cambridge University Press, Cambridge, 1982).
- [13] G. Bodo, A. Mignone, and R. Rosner, *Phys. Rev. E* **70**, 036304 (2004).
- [14] M. Tabak, *Phys. Plasmas* **1**, 1626 (1994).
- [15] K. A. Tanaka, R. Kodama, K. Mima, Y. Kitagawa, H. Fujita, N. Miyanaga, K. Nagai, T. Norimatsu, T. Sato, Y. Sentoku, K. Shigemori, A. Sunahara, T. Shozaki, M. Tanpo, S. Tohyama, T. Yabuuchi, J. Zheng, T. Yamanaka, P. A. Norreys, R. Evanse, M. Zepf, K. Krushelnic, A. Dangor, R. Stephens, S. Hatchett, M. Tabak, and R. Turner, *Phys. Plasmas* **10**, 1925 (2003).
- [16] S. V. Bulanov, F. Pegoraro, and A. S. Sakharov, *Phys. Fluids B* **4**, 2499 (1992).
- [17] A. Das, *Plasma Phys. Controlled Fusion* **41**, A531 (1999).
- [18] A. Das and P. Kaw, *Phys. Plasmas* **8**, 4518 (2001).
- [19] D. Jovanovic and F. Pegoraro, *Phys. Plasmas* **7**, 889 (2000).
- [20] S. Sundar and A. Das, *Phys. Plasmas* **17**, 022101 (2010).
- [21] Sita Sundar, Amita Das, and Predhiman Kaw *Phys. Plasmas* **19**, 052105 (2012).
- [22] Pritchett, P. L., and F. V. Coroniti, *J. Geophys. Res.* **89(A1)**, 168 (1984).

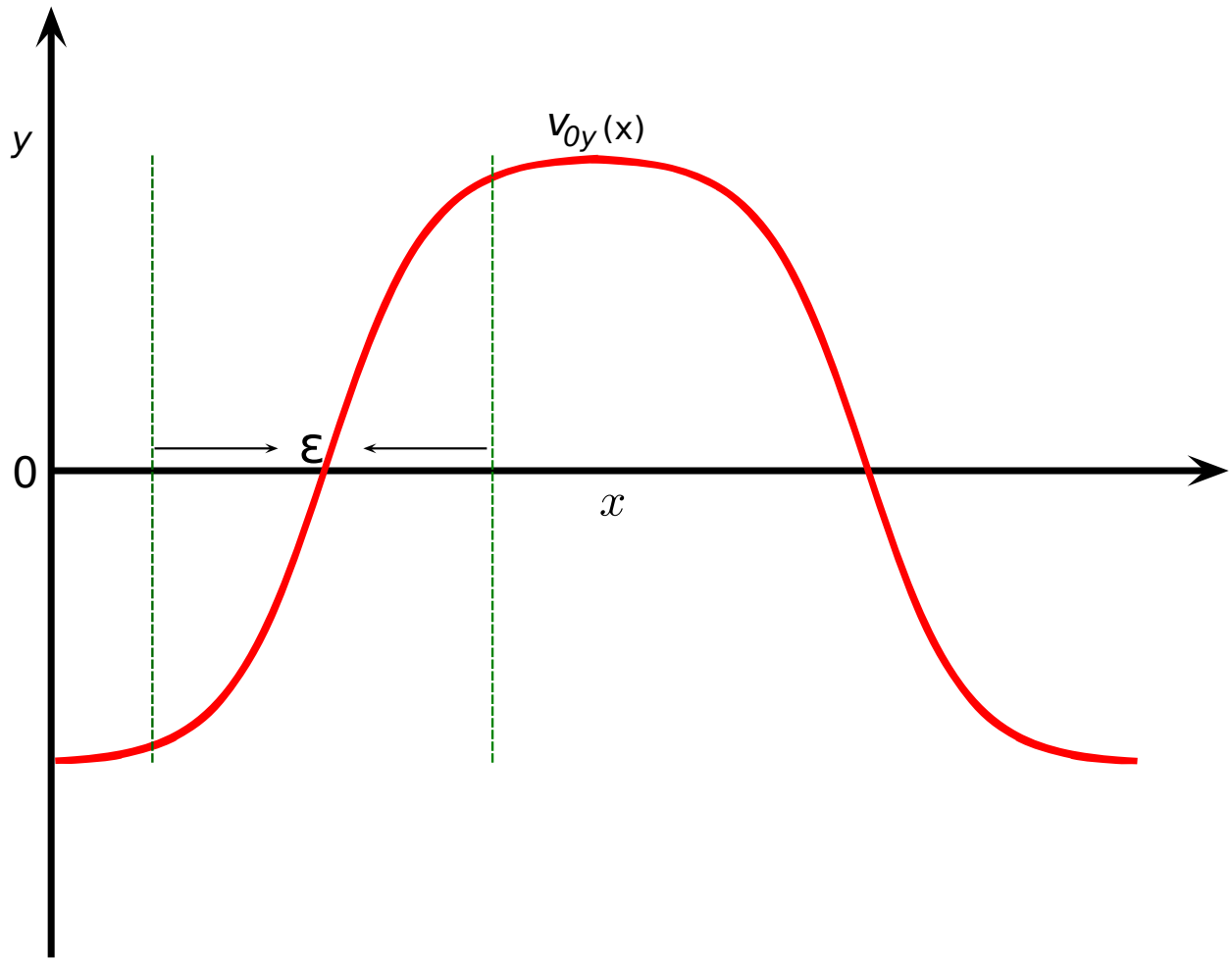


FIG. 1: The schematic of system in present article. Initially electrons flow with double tangent hyperbolic along y -axis.

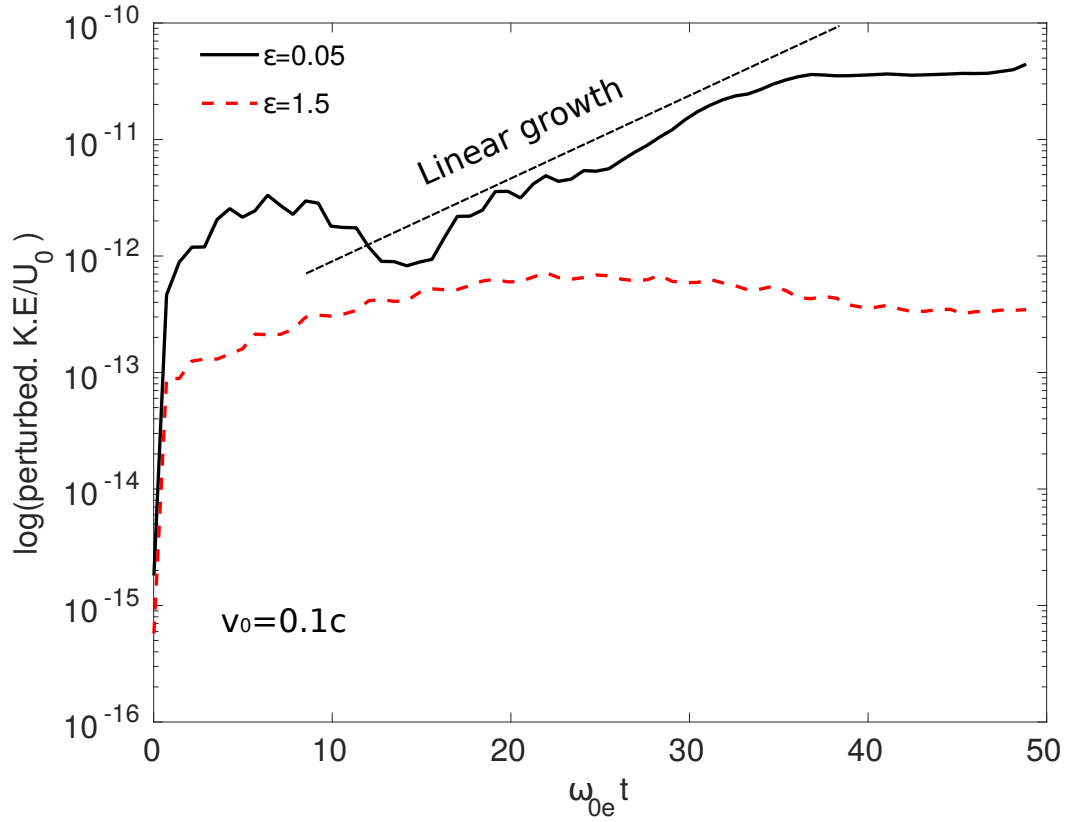


FIG. 2: Time evolution of perturbed kinetic energy where $u_0 = (mec\omega_{0e}/e)^2$ for case (a) (black color, solid line) and case(b) (red color, solid line). The slope gives linear growth rate of KH instability.

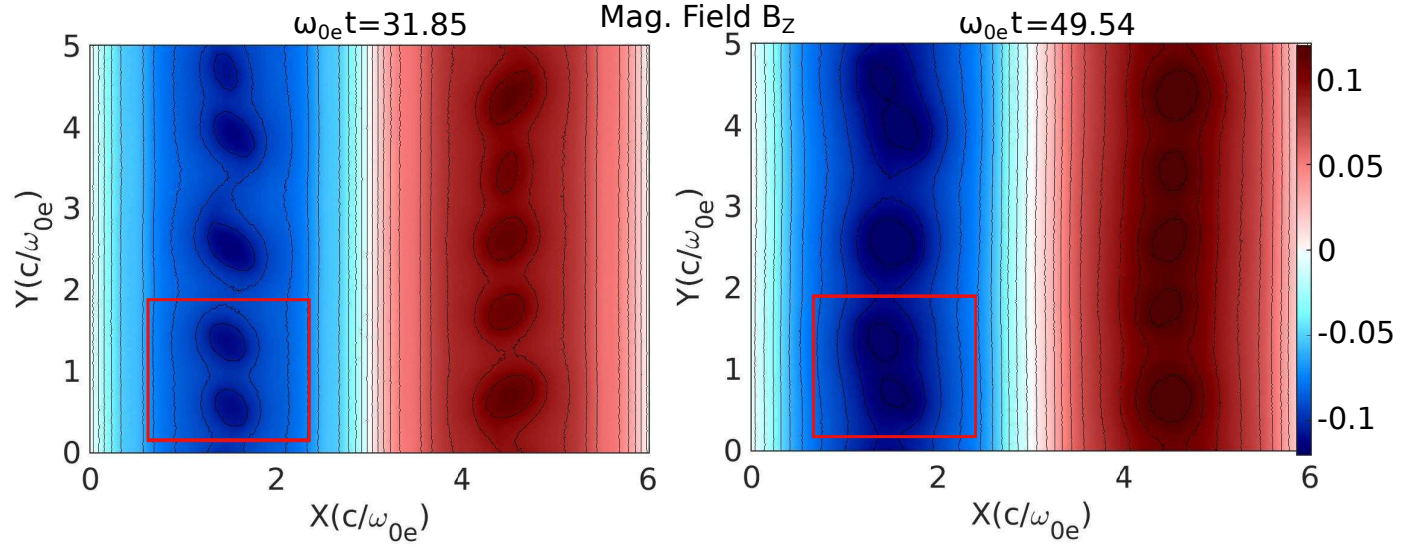


FIG. 3: Time evolution of z -component of magnetic field $B_Z = B_Z/(mec\omega_{0e}/e)$ for case (a) at time $\omega_{0e}t=31.85$ and 49.54. The vortices in magnetic field are highlighted by red box ($31.85\omega_{0e}t$) which merge at later time $\omega_{0e}t=49.54$ (highlighted by red box).

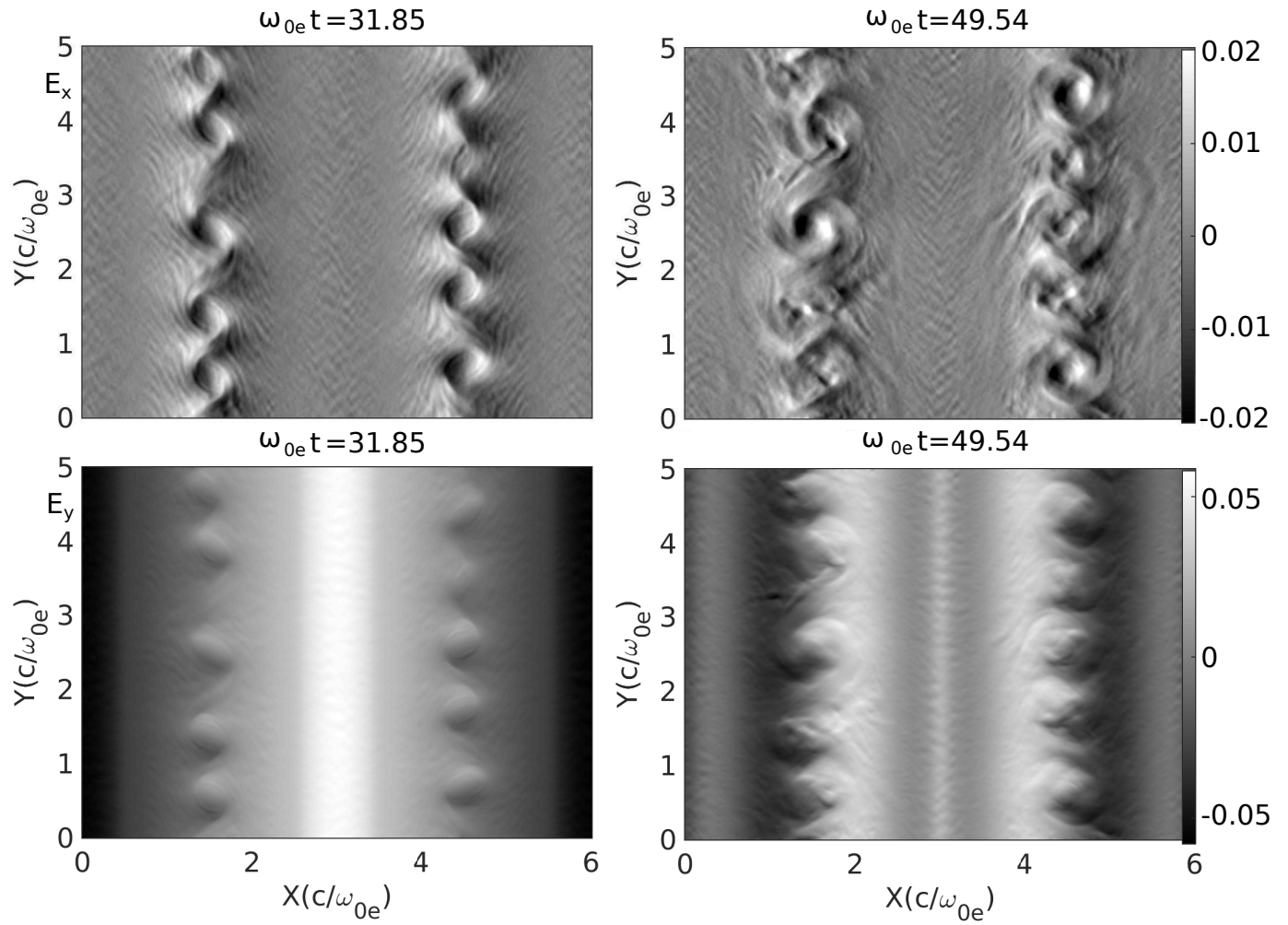


FIG. 4: The time evolution of electric field: first row shows the x-component of electric field $E_x = E_x/(mec\omega_{0e}/e)$ and second row shows y-component of electric field

$$E_y = E_y/(mec\omega_{0e}/e) \text{ for case (a) } (V_0 = 0.1c, \varepsilon = 0.05d_e.)$$

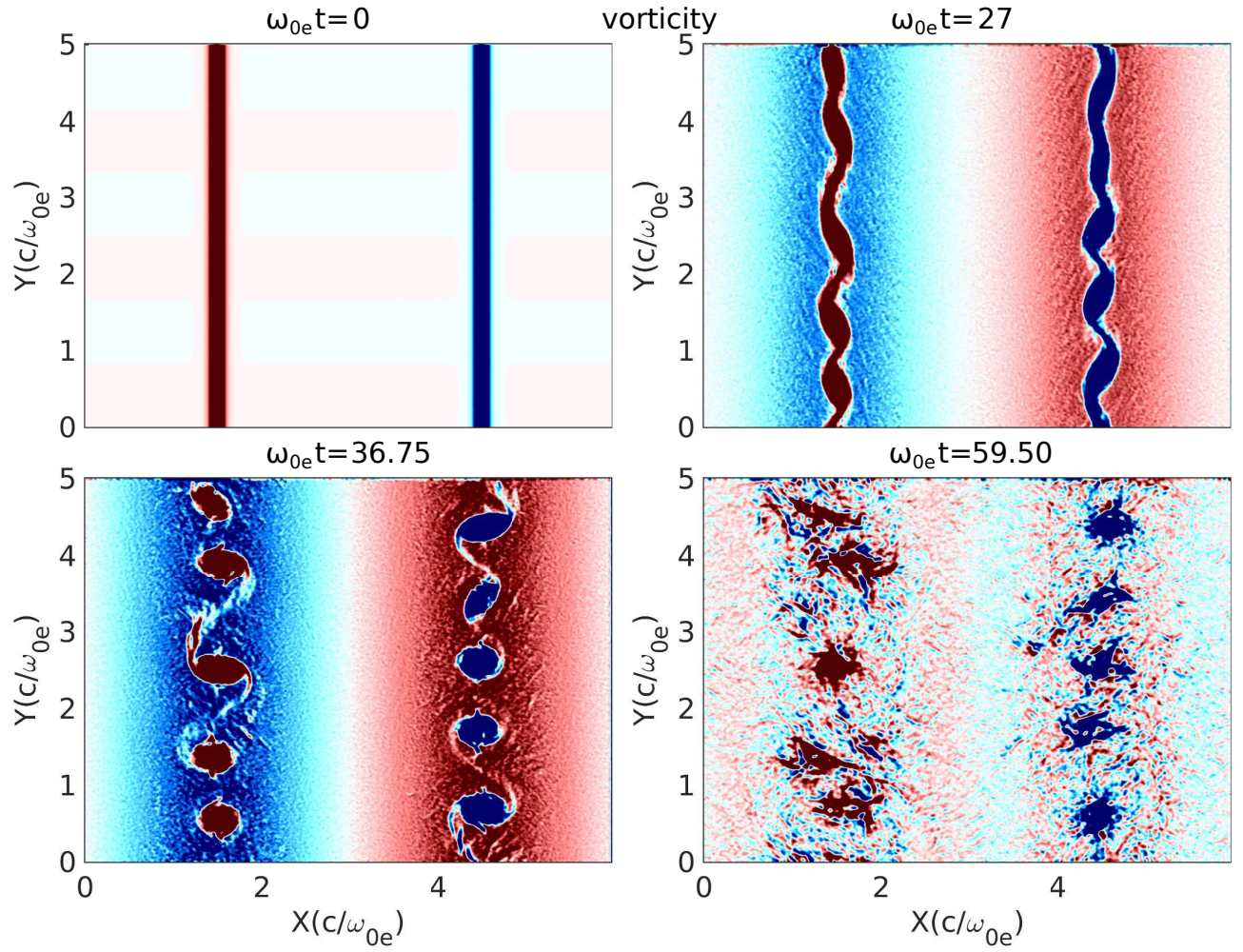


FIG. 5: The time evolution of vorticity $((\nabla \times V)/\omega_{0e})$ calculated from velocity field for case (a) ($V_0 = 0.1c$, $\varepsilon = 0.05d_e$) which shows merging of vortices with time and turbulence stage of KH instability.

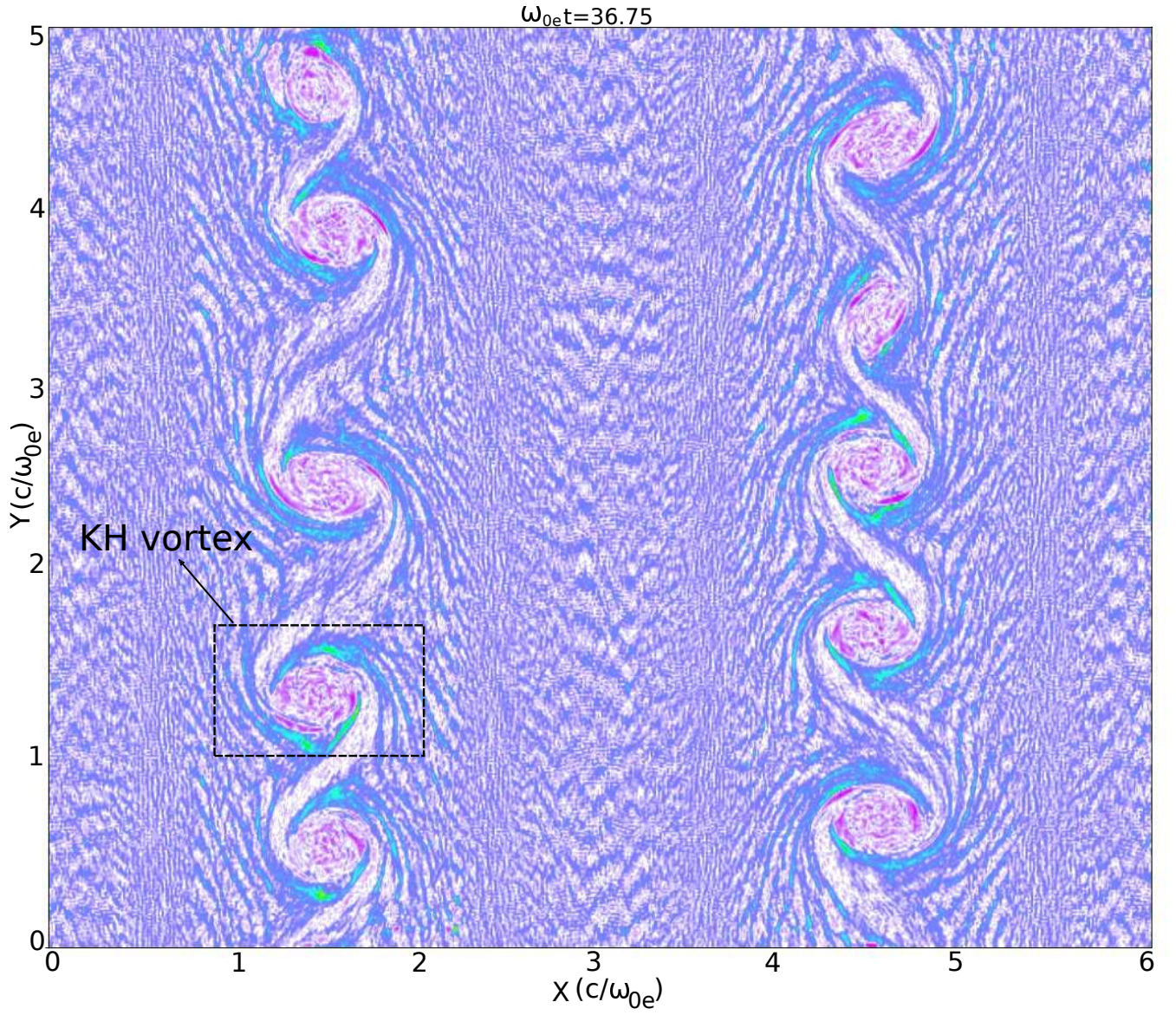


FIG. 6: Formation of KH vortex (highlighted by black box) in electron density $n_e = n_e/n_{0i}$ at time $\omega_{0e}t = 36.75$ for case (a).

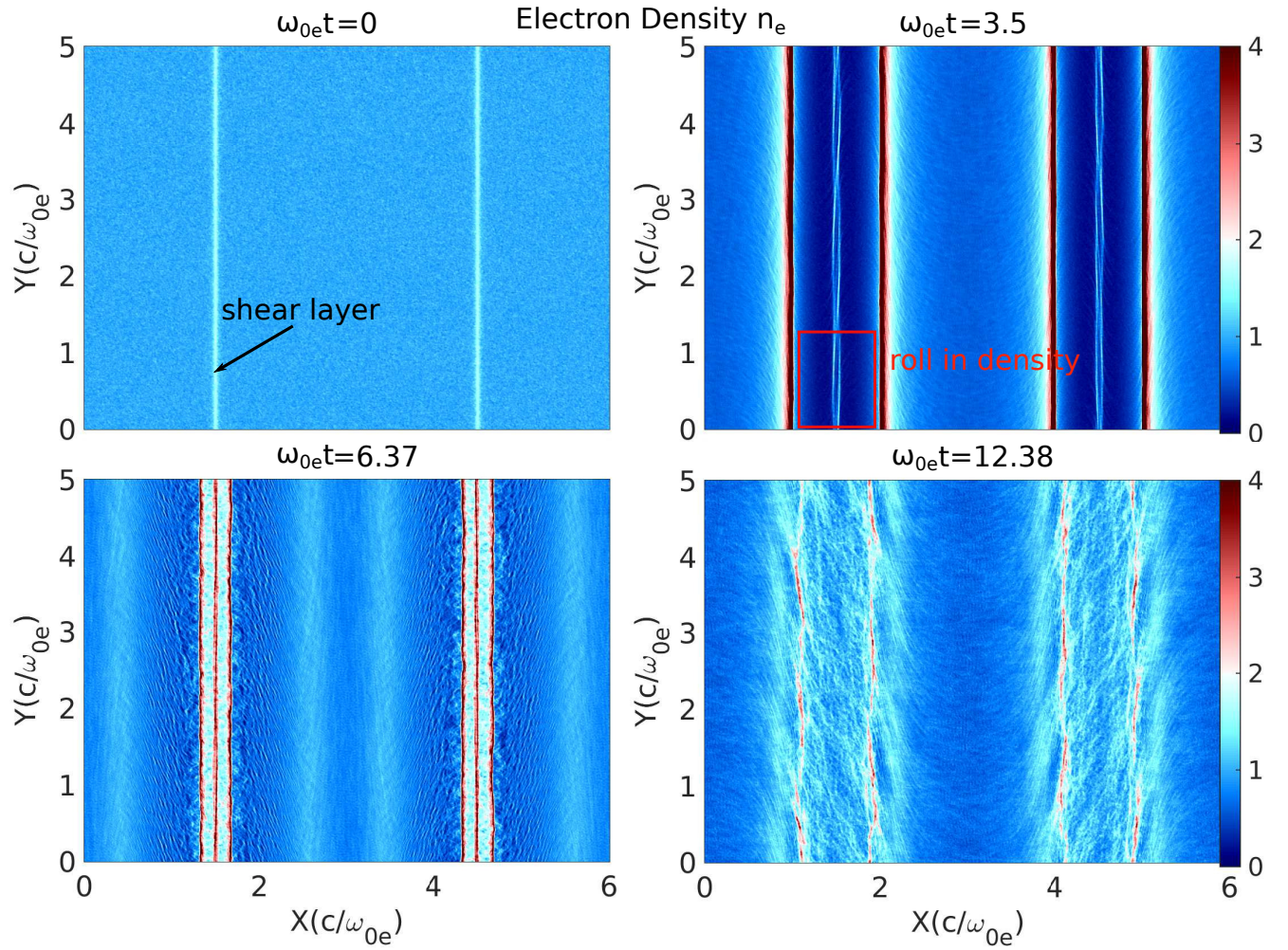


FIG. 7: The time evolution of electron density $n_e = n_e/n_{0i}$ for case (c) that shows the roll in density at time $\omega_{0e}t=3.5$ at shear layer (highlighted by red box) which is signature of KH instability. The compression and rarefaction in density can be also seen.

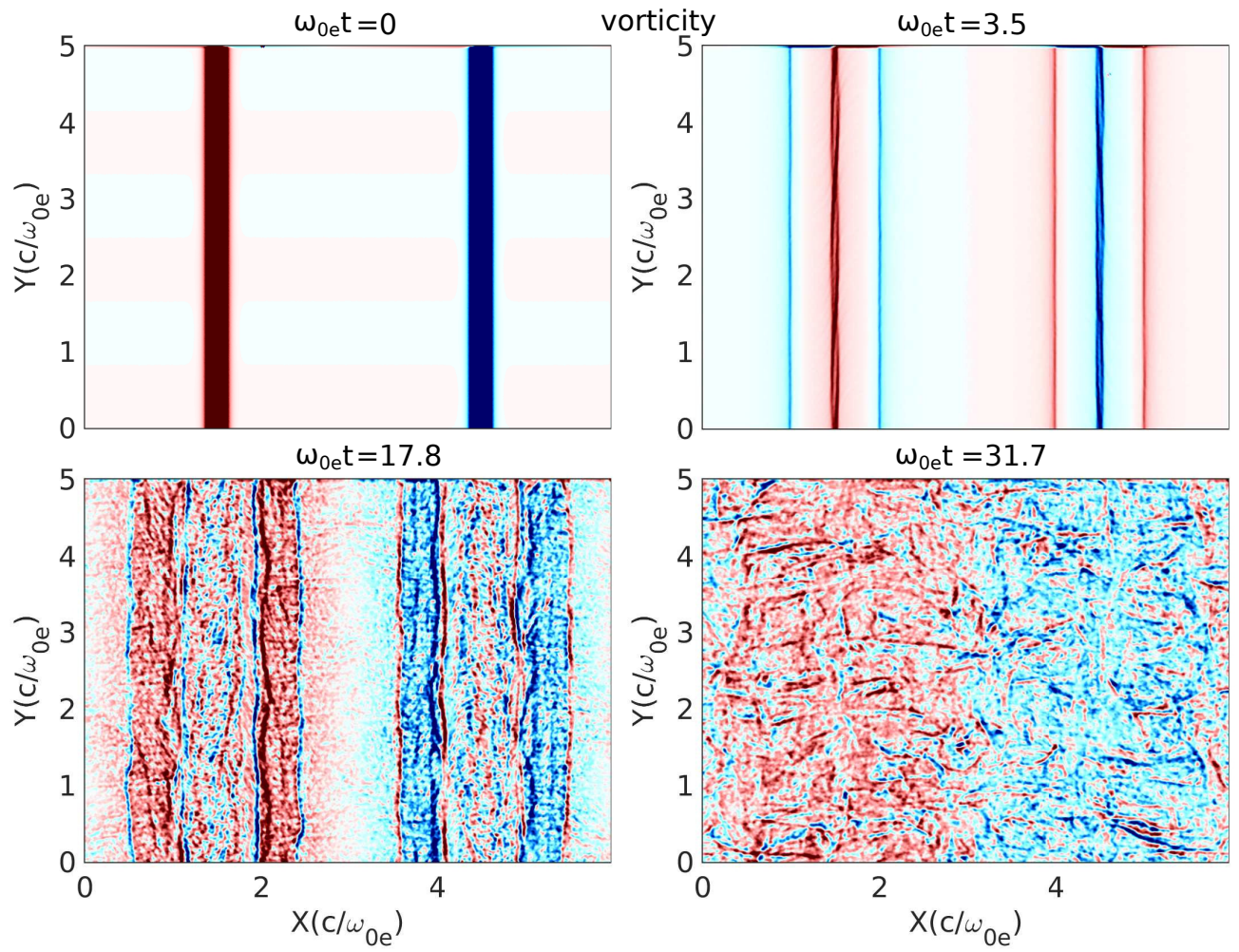


FIG. 8: The time evolution of vorticity ($\nabla \times V$) calculated from velocity field for case (b).

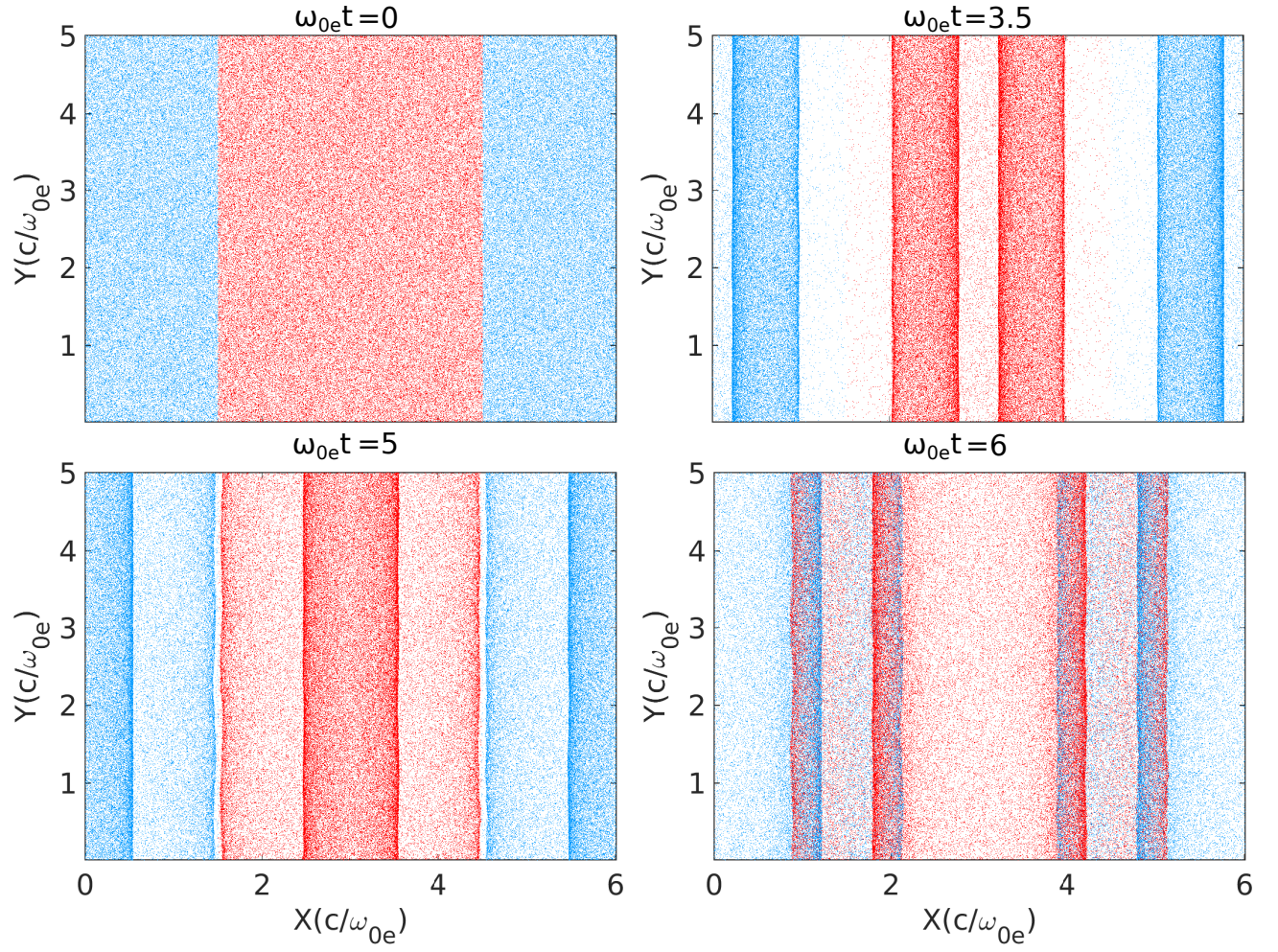


FIG. 9: Particle picture of 2-D electron electron velocity shear configuration for case (d) which shows transverse oscillations of particles with time.

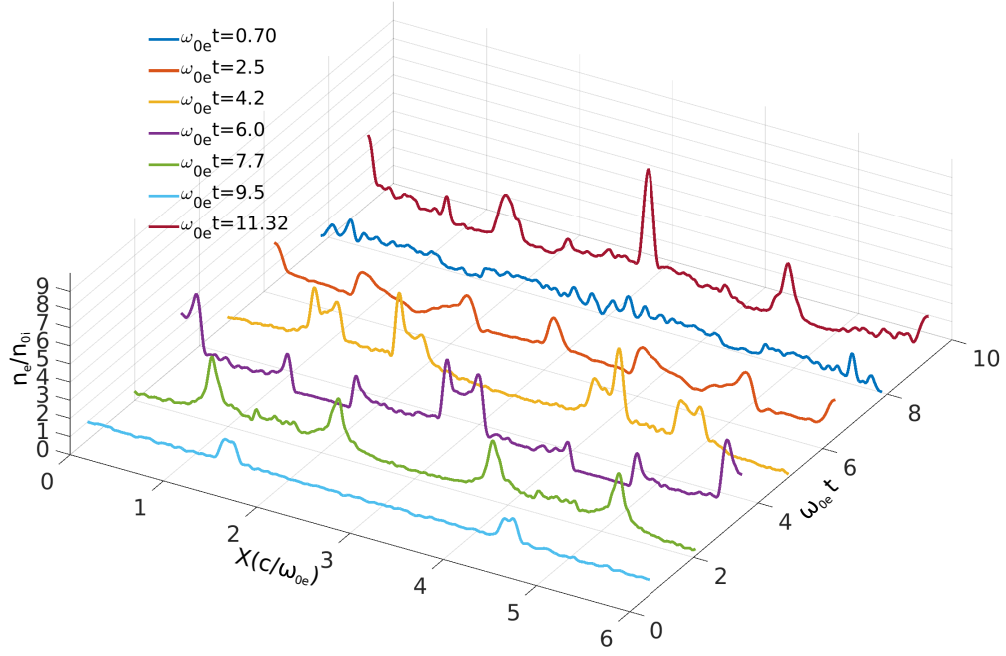


FIG. 10: Time evolution of electron density diagnosed at $y = 2.5c/\omega_{e0}$ for $V_0 = 0.9c$, $\varepsilon = 0.05d_e$: This figure shows non-linear large amplitude electrostatic oscillations which break in later time.

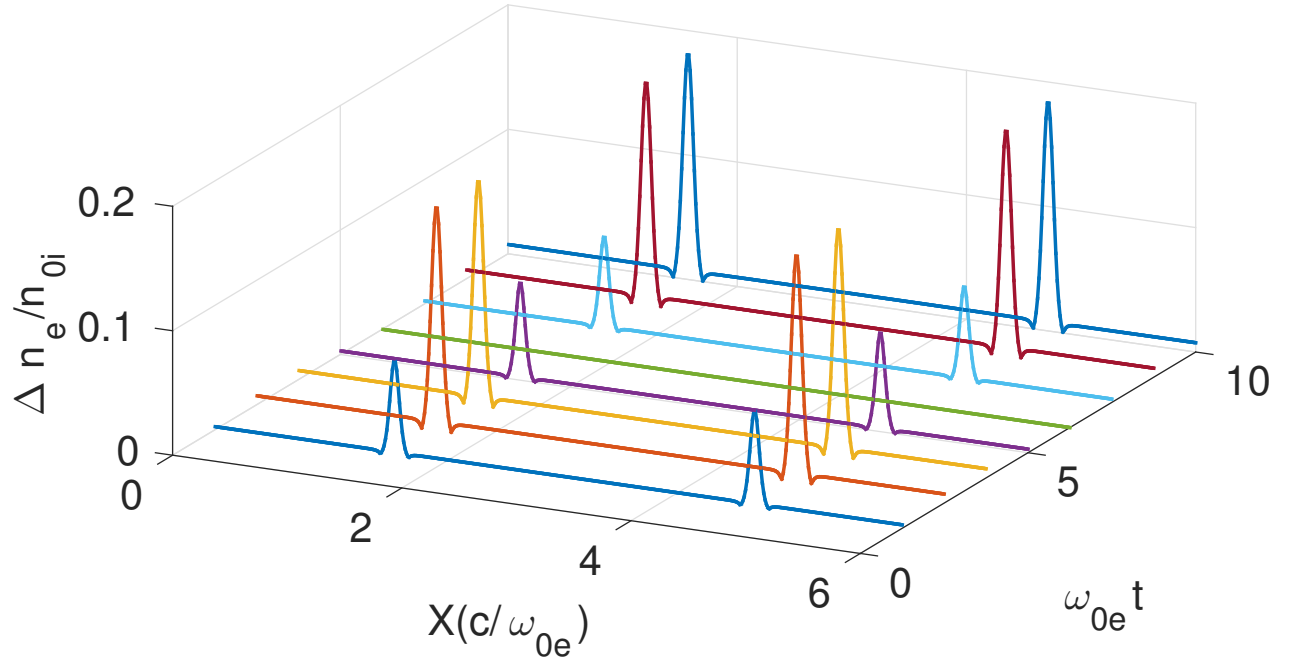


FIG. 11: Time evolution of perturbed electron density $\Delta n_e = |(n_e - n_{e0})|$ obtained from 1D model diagnosed at $y = 2.5c/\omega_{e0}$ for $V_0 = 0.1c$, $\varepsilon = 0.05d_e$: This figure shows small amplitude electrostatic oscillations in presence of inhomogeneous magnetic field $B(x)$.

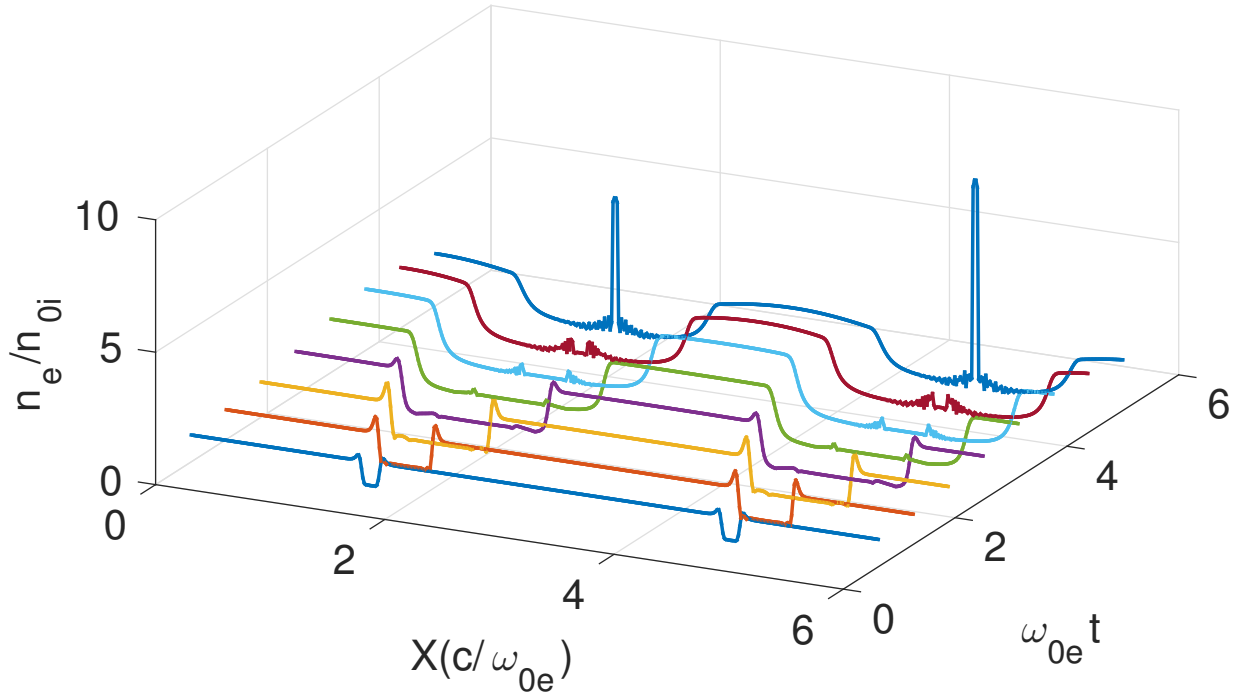


FIG. 12: Time evolution of perturbed electron density n_e/n_{0i} obtained from 1D model diagnosed at $y = 2.5c/\omega_{e0}$ for $V_0 = 0.9c$, $\varepsilon = 0.05d_e$: This figure shows non-linear large amplitude electrostatic oscillations which break in later time.

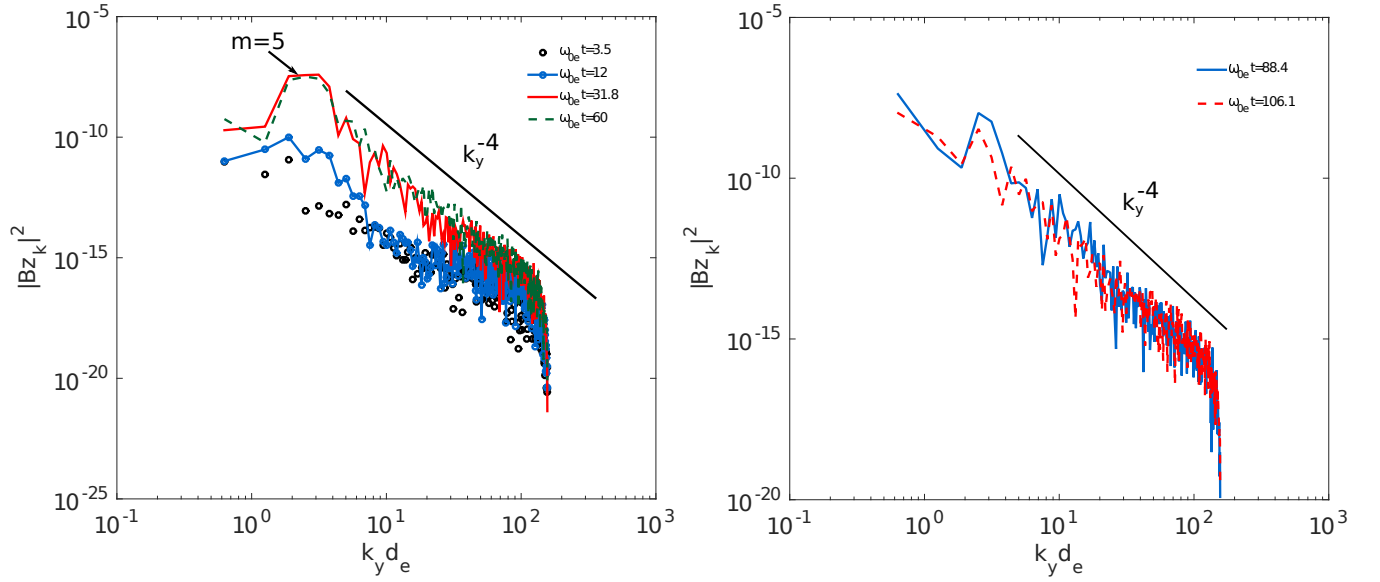


FIG. 13: Longitudinal spectrum of magnetic field energy $|Bz_k|^2 = |Bz_k/(mec\omega_{0e}/e)|^2$ with time for weakly relativistic case ($V_0 = 0.1c$, $\varepsilon = 0.05d_e$). (a) spectra of magnetic field up at early time where we can see the domination of power corresponding to mode $m=5$ (where $m=L_y k_y/2\pi$) (b) spectra in turbulent stage.

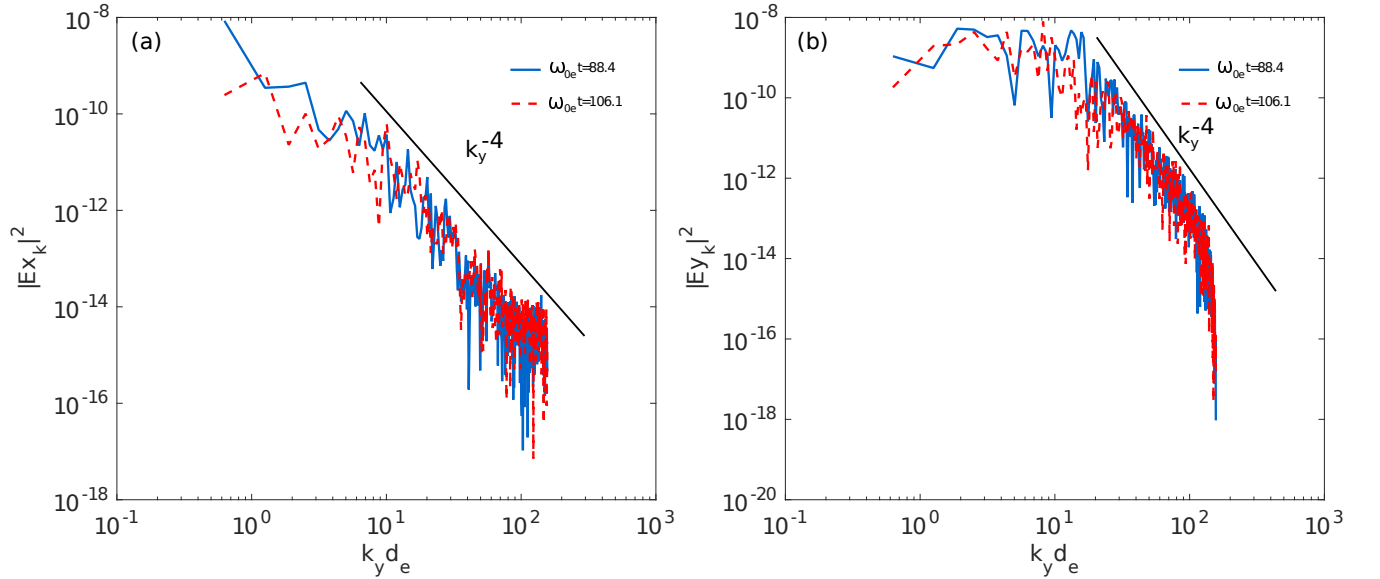


FIG. 14: Longitudinal spectrum of electric field energy with time for weakly relativistic case ($V_0 = 0.1c$, $\varepsilon = 0.05d_e$). (a) spectra of x-component of electric field energy $|Ex_k|^2 = |Ex_k/(mec\omega_{0e}/e)|^2$ (b) spectra of y-component of electric field energy $|Ey_k|^2 = |Ey_k/(mec\omega_{0e}/e)|^2$.

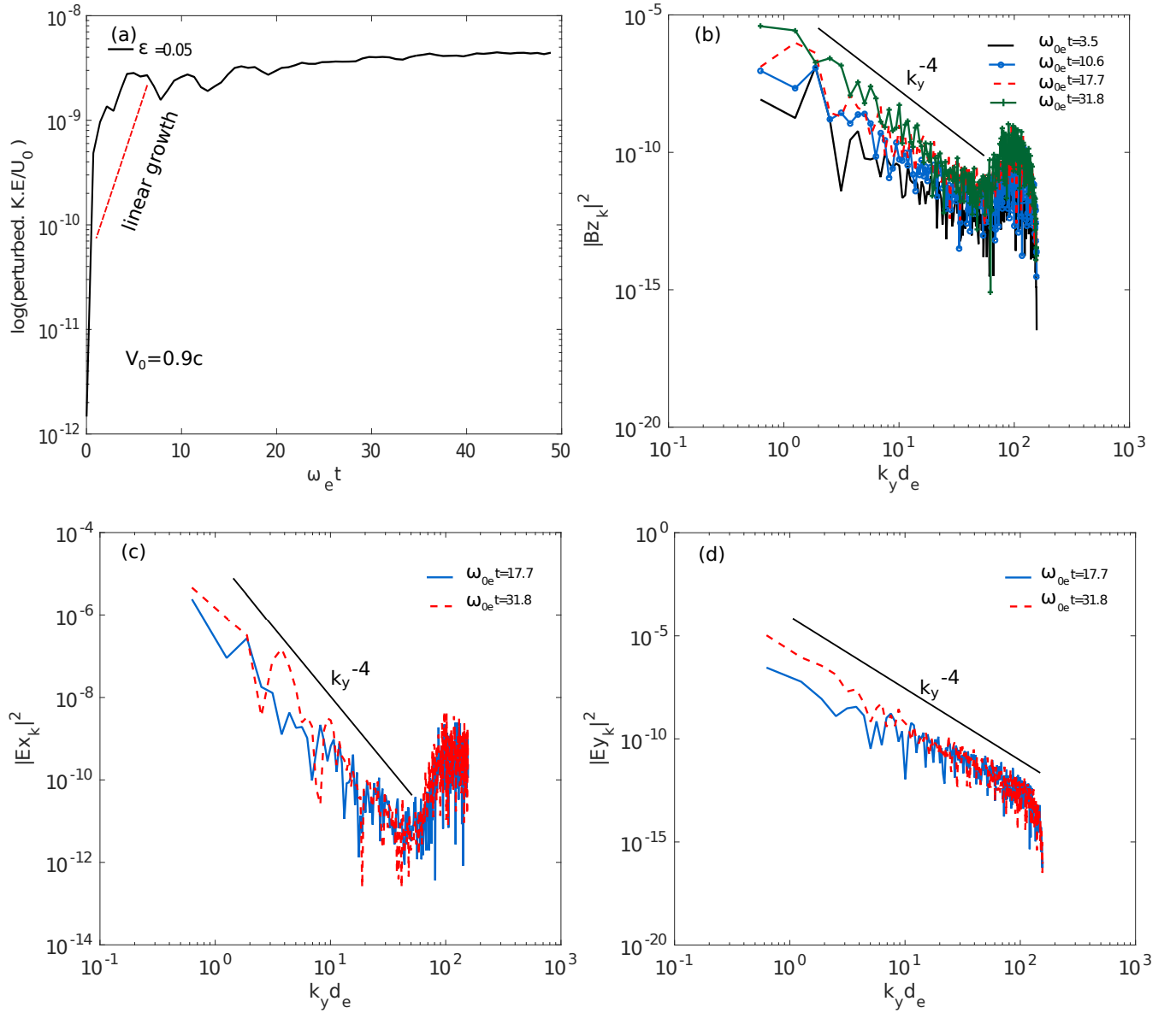


FIG. 15: perturbed kinetic energy and fields spectra for ultra-relativistic case ($V_0 = 0.9c$, $\varepsilon = 0.05$ c/ω_{0e}) (a) Time evolution of perturbed kinetic energy (b) longitudinal spectra of magnetic field energy $|Bz_k|^2 = |Bz_k/(mec\omega_{0e}/e)|^2$ (c) longitudinal spectra of x-component of electric field energy $|Ex_k|^2 = |Ex_k/(mec\omega_{0e}/e)|^2$ (d) spectra of y-component of electric field energy $|Ey_k|^2 = |Ey_k/(mec\omega_{0e}/e)|^2$.